

## Deliverable D 3.10 Critical material and lining (geometry, layout...) parameters for the structure's lifespan

Document type	<b>Deliverable D 3.10</b>
Document Version / Status	<b>1.5</b>
Primary Authors	<b>Alain GASSER, <a href="mailto:alain.gasser@univ-orleans.fr">alain.gasser@univ-orleans.fr</a>, UORL</b>
Distribution Level	<b>PU (Public)</b>
Project Acronym	<b>ATHOR</b>
Project Title	<b>Advanced THERmomechanical multiscale mOdelling of Refractory linings</b>
Grant Agreement Number	<b>764987</b>
Project Website	<b><a href="http://www.etn-athor.eu">www.etn-athor.eu</a></b>
Project Coordinator	<b>Marc Huger, <a href="mailto:marc.huger@unilim.fr">marc.huger@unilim.fr</a>, UNILIM</b>
Document Contributors	<b>Alain GASSER, <a href="mailto:alain.gasser@univ-orleans.fr">alain.gasser@univ-orleans.fr</a>, UORL Mahmoud ALI, <a href="mailto:mahmoud.ali@univ-orleans.fr">mahmoud.ali@univ-orleans.fr</a>, UORL</b>

### History of Changes

Version	Date	Author (Organization)	Change	Page
1.1	10/01/2022	Mahmoud ALI (UORL)	Creation of the first version	All
1.2	12/01/2022	Alain GASSER (UORL)	Revision	All
1.3	24/01/2022	Mahmoud ALI (UORL)	Revision	All
1.4	25/01/2022	Alain GASSER (UORL) Mahmoud ALI (UORL)	Revision	11
1.5	14/03/2022	Glyn DERRICK (UNILIM) Marc HUGER (UNILIM)	English and formatting check Final check	All

### TABLE OF CONTENTS

1 INTRODUCTION.....	1
2 PHYSICAL MODEL AND MATERIALS .....	2
3 PROCESS DESCRIPTION .....	3
4 THERMAL AND MECHANICAL MODELLING .....	3
5 RESULTS AND DISCUSSION .....	5
5.1 Temperature fields.....	5
5.2 Joints closure and reopening.....	7
5.3 Stress fields.....	8
6 CONCLUSION .....	19
7 REFERENCES.....	19

## 1 Introduction

The present deliverable is dedicated to transient nonlinear thermo-mechanical modelling of an industrial steel ladle. The constitutive homogeneous material models of masonry with dry or mortar joints, developed and validated at University of Orléans within the framework of ATHOR project, were used to represent the different masonry linings in the steel ladle. Parametric studies investigating the impacts of dry joints thickness, dry joints behaviour and constitutive material models used for the different linings of the ladle were carried out. Details regarding the physical model of the studied ladle, materials and masonry type used for each

linings are given in section 2. Descriptions of a typical thermal cycle of steel ladles and related cyclic thermal heating and cooling are presented in section 3. Details about the transient heat transfer analysis of the steel ladle and related thermal boundary conditions, governing equations and mechanical boundary conditions are described in section 4. The results and discussions of the transient heat transfer and thermomechanical analysis are presented in section 5. The conclusion of the present deliverable is given in section 6.

## 2 Physical model and materials

Refractories are the best candidate materials for the steel ladle application due to their low thermal conductivity as well as their thermal, chemical and mechanical stability at high temperatures. To meet the mechanical, thermal and operational requirements, different refractory layers are used for the construction of the ladle. Each layer has a specific purpose and has unique thermo physical and mechanical properties. In the studied ladle, the different layers include a working lining, a safety lining (also called permanent lining), an insulation layer and a steel shell (see Figure 1). The working lining is made of mortarless refractory masonry. The safety lining is built up with a dense refractory masonry with mortar joints with low thermal conductivity. The insulation layer (with 5 mm thickness) is made of a porous material with very low thermal conductivity.

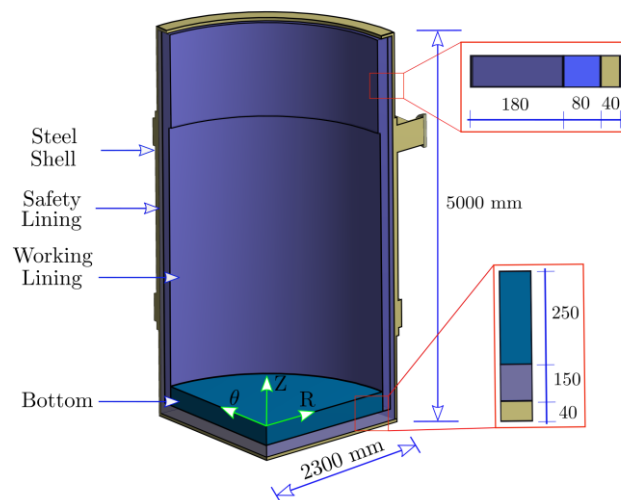


**Figure 1: Schematic of a simplified steel ladle showing the different layers, all dimensions are in mm. The 5 mm thickness insulation layer is not represented.**

The mechanical and thermo physical properties of each layer are reported in Table 1 where  $\rho$  is the density,  $C_p$  is the specific heat,  $k$  is the thermal conductivity,  $Y$  is the Young's modulus, and CTE is the coefficient of thermal expansion. The thermo-physical and mechanical properties of the working lining and the bottom are reported in deliverable 3.9 (alumina spinel). For the safety lining, the shear failure criteria of the brick/mortar interface were determined using slanted shear tests (similar to those performed by Brulin et al. [1]). The cohesion of the brick/mortar interface is equal to 0.73 MPa at 20 °C and 1.26 MPa at 600 °C. The internal friction angle is equal to 40° and Young's modulus of the mortar is equal to 1000 MPa (assumed due to lack of data). The mechanical and thermophysical properties of the working lining (alumina spinel) are reported in deliverable 3.6.

A typical industrial scale steel ladle has complex geometry and is composed of refractory linings, steel construction components, valves, purging plugs, lifting points, etc. In order to reduce the computational time, some detailed features such as valves, nozzles, and purging plugs have been neglected. In addition, due to the symmetry of the studied ladle, only one quarter has been considered. The simplified physical model of the studied steel ladle is presented in Figure 1. The height and diameter of the ladle are 5 and 4.6 m, respectively. The thickness of each layer is given in mm and reported in Figure 1 (except the insulation layer, 5 mm between the steel shell and the safety lining).

**Table 1: Thermo-physical and mechanical properties of the materials used for the different layers in the studied steel ladle.**

Lining	Layer	Properties		References	
Steel shell	Steel shell	$\rho$ (kg/m <sup>3</sup> )	7840	[2]–[4]	
		k (W/m.K)	47.3 at 200 °C		
			42.3 at 350 °C		
			37.3 at 500 °C		
		$C_p$ (J/kg.K)	30 at 200 °C 666 at 500 °C		
Y (GPa)	210 at 20 °C 170 at 400 °C				
		CTE (10 <sup>-6</sup> K <sup>-1</sup> )	12		
Safety lining	Bottom and wall bricks (dense layer)	$\rho$ (kg/m <sup>3</sup> )	2660	[2], [4]	
		k (W/m.K)	2.6 at 400 °C 2.1 at 800 °C 2 at 1200 °C		
			$C_p$ (J/kg.K)		8900 at 200 °C 1144 at 1200 °C
			Y (GPa)		4.5 at 800 °C 3.5 at 1000 °C 1 at 1200 °C
					CTE (10 <sup>-6</sup> K <sup>-1</sup> )
Insulation	Bottom and wall insulation (porous layer)	$\rho$ (kg/m <sup>3</sup> )	510	[2]–[4]	
		k (W/m.K)	0.15 at 250 °C 0.25 at 800 °C 0.34 at 1350 °C		
			$C_p$ (J/kg.K)		1047
			Y (GPa)		0.3
					CTE (10 <sup>-6</sup> K <sup>-1</sup> )

### 3 Process description

In the steel industry, steel ladles are used to transport liquid steel from electric arc furnaces or converters to continuous casting machines. In addition, they are used as refining units. While holding liquid steel, other processes occur in parallel such as degassing and alloying. During these processes, the ladle is exposed to different thermal and mechanical operating conditions. A typical thermal cycle of steel ladle refractory linings includes:

- Step 1: preheating the working lining using natural gas burner (to around 1400 °C).
- Step 2: slight temperature decrease due to thermal losses while moving from the preheating device to the converter and waiting for liquid steel tapping.
- Step 3: sudden temperature increase due to tapping liquid steel into the ladle.
- Step 4: gradual temperature drop due to teeming liquid steel out of the ladle, thermal losses during linings check and, if required, lining repairs.

Further details on the thermal modelling of the steel ladle thermal cycle, governing equations and boundary conditions of each step are given in section 4.

### 4 Thermal and mechanical modelling

During the previously described thermal cycle, the temperature distribution ( $T$ ) of the ladle varies with time ( $t$ ) and can be obtained by solving the transient form of the energy equation given by [5]:

$$\rho C_p \frac{\partial T}{\partial t} - \text{div}(\overrightarrow{k \text{grad}(T)}) = 0 \quad \text{Equation 1}$$

The initial temperature ( $T_i$ ) of all material layers in the ladle is assumed to be the same as the ambient temperature. Under this assumption, the initial boundary conditions can be expressed using [5]:

$$T(R, \theta, Z, t = 0) = T_i = 20 \text{ }^\circ\text{C} \quad \text{Equation 2}$$

During the first step, a natural gas burner is used to heat the inner surfaces of the ladle from the ambient temperature to around 1400 °C. The time period for this step is approximately 6.5 h [2], [4], [6]. The dominant heat transfer mode to the lining surfaces is radiation with only conduction occurring within the thickness of the different layers. Modelling radiative heat transfer between the burner and the lining surfaces requires solving the full Navier-Stokes and the energy conservation equations that govern the combustion process. This necessitates long computation times and lies outside the scope of the present work. A simple approach that can reasonably simulate the transient thermal response of the ladle during preheating is to consider convective heat transfer between a heat transfer fluid (HTF) and lining surfaces. The temperature of the HTF ( $T_{hf}$ ) is assumed to be 1600 °C. The convective heat flux on the internal surfaces ( $q_{i1}$ ) of the ladle can be expressed as [5]:

$$\begin{aligned} q_{i1} &= h_{i1}(T_{hf} - T(R, \theta, Z, t)) \\ \frac{\partial T_{i1}}{\partial \vec{n}} &= h_{i1}(T_{hf} - T(R, \theta, Z, t))\vec{n} \end{aligned} \quad \text{Equation 3}$$

where  $h_{i1}$  is the convective heat transfer coefficient during step 1 (its value is temperature dependent, see Figure 2-a) and  $\vec{n}$  is the outward normal to the surface. The radiative and convective thermal losses ( $q_e$ ) from the outer surfaces of the steel shell to the ambient can be written as [5]:

$$q_e = h_e(T_{sh}(R, \theta, Z, t) - T_{amb}) + \epsilon S(T_{sh}^4(R, \theta, Z, t) - T_{amb}^4) \quad \text{Equation 4}$$

where  $T_{amb}$ ,  $\epsilon$ ,  $S$ , and  $T_{sh}$  are the ambient temperature (20 °C), emissivity (0.8), Stefan-Boltzmann constant, and the steel shell outer surface temperature, respectively.  $h_e$  is the convective heat transfer coefficient between the steel shell outer surface and the ambient (10 W/m<sup>2</sup> K). This boundary condition has been applied to the external surfaces during all steps of the thermal cycle of the ladle.

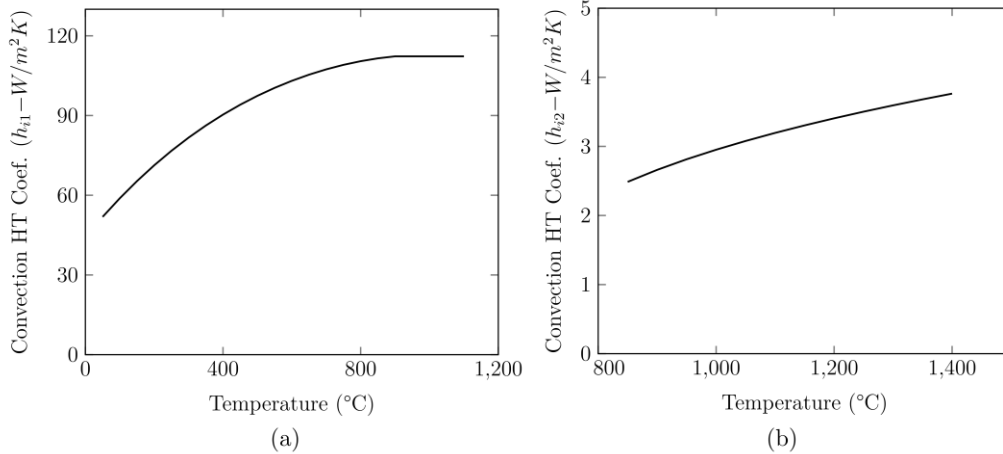


**Figure 2: Convection heat transfer coefficient variations vs. temperature used for (a) the first step and (b) the second step of the ladle thermal cycle [6].**

During step 2, the steel ladle is moved from the heating device to the converter or to the electric arc furnace and waits to receive the liquid steel. The duration of this step can be up to 15 min. During this period, the inner and outer surfaces of the ladle exchange heat with the environment by convection and radiation mechanisms. Heat losses of the external surface are expressed by equation 5, whereas heat losses from the internal surfaces ( $q_{i2}$ ) are written as [6]:

$$q_{i2} = h_{i2}(T_i(R, \theta, Z, t) - T_{env.}) + \epsilon S(T_i^4(R, \theta, Z, t) - T_{env.}^4) \quad \text{Equation 5}$$

with  $h_{i2}$  (its value is temperature dependent, see Figure 2-b),  $T_i$ , and  $T_{env}$ , denoting the heat transfer coefficient during step 2, internal surfaces temperature, and environmental temperature (900 °C, the hot air inside the ladle), respectively.

After step 2, liquid steel ( $T_s = 1650$  °C) is poured into the steel ladle, leading to a sudden increase in lining temperature (thermal shock). During this step, other processes may occur in parallel (degassing, alloying, etc.), and the total duration of this step is assumed to be 2 h. During this period, heat is transferred from the liquid steel to the linings mainly by convection [7]. The convective heat flux on the internal surfaces ( $q_{i3}$ ) can be expressed as:

$$q_{i3} = h_s(T_s - T_i(R, \theta, Z, t)) \quad \text{Equation 6}$$

Where  $h_s$  is the convective heat transfer coefficient between the liquid steel and the inner surfaces of the ladle. A very high value of  $h_s$  (2000 W/m<sup>2</sup> K) was used in order to obtain the sudden temperature increase of the lining. This value is taken from [2].

Regarding the last step of the thermal cycle (step 4), liquid steel is drained out of the ladle. The temperatures of the ladle's internal and external surface decrease gradually due to thermal losses to the ambient. The heat losses during this step are considered similar to those of step 2. It should be noted that the heating and cooling rates during the four steps of the thermal cycle are different, as, according to Equations (3), (5) and (6), they are functions of the temperature of the internal surfaces. For example, in the beginning of the first preheating (1<sup>st</sup> step of 1<sup>st</sup> thermal cycle), the heating rate is very high as compared to the heating rate at the end of the same step.

The thermal model for steel ladle shown in Figure 1 has been developed using Abaqus software. Then weak thermomechanical coupling was used for the thermomechanical analysis. The computed temperature distributions have been used as a thermal load for the transient thermomechanical models. Symmetry boundary conditions have been applied to the symmetric planes of the physical model of the ladle. The outer surface of the steel shell's bottom was assumed to be fixed in the vertical direction (z-direction in Figure 1). The weight and hydro-static pressure of the liquid steel were neglected as their impacts on resulting stresses are very small (around 1 MPa) as compared to the impact of the thermal expansion of the bricks (around 100 MPa in some cases). The frictional interactions between the different layers of the ladle are considered in the numerical model using surface to surface contact in Abaqus (coefficient of friction 0.5). Several constitutive material models were used for describing the mechanical behaviours of the working (masonry with dry joints) and the safety (masonry with mortar joints) linings. More details about the employed material models are given later in this deliverable.

## 5 Results and discussion

### 5.1 TEMPERATURE FIELDS

Time variations of the temperature of the working lining hot face (HF, surface in contact with liquid steel), cold face (CF, surface in contact with the safety lining) and the steel shell outer surfaces (bottom and wall) during the first three complete production cycles are shown in Figure 3. As explained earlier, during step 1 (a to b), heat is transferred by forced convection from a heat transfer fluid at 1600 °C to the working lining (initial temperature is about 20 °C). As a result, the temperature of the working lining increases gradually from room temperature to around 1400 °C. The steel ladle is then transported, in step 2, from the heating device to the converter or electric arc furnace while losing heat to the environment by convection and radiation mechanisms (b to c). This leads to a drop in temperature to around 1200 °C. During step 3 (c to d), liquid steel (at around 1650 °C) is tapped into the ladle, resulting in a sudden increase in the temperature. In step 4, the end of the thermal cycle (d to e), the working lining temperature decreases gradually. The observed decrease in temperature is due to the teeming of liquid steel and the heat losses (by convection and radiation mechanisms) from external and internal surfaces of the ladle to the ambient. Then, the first thermal cycle is repeated twice (except for the preheating from ambient temperature).

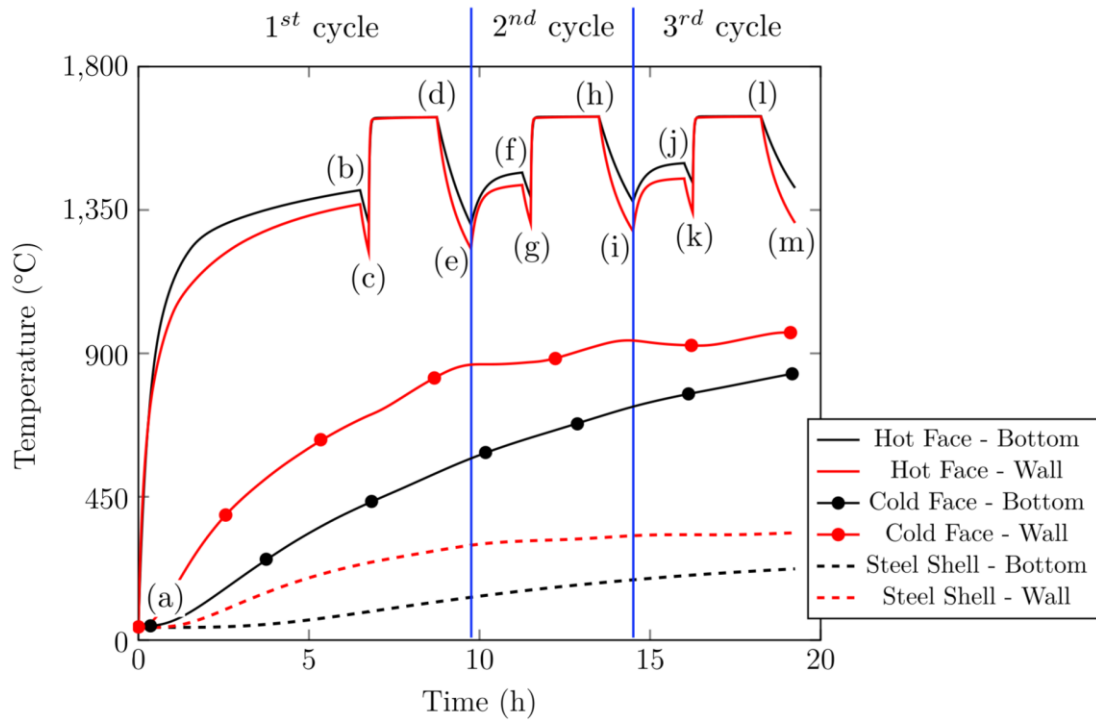


**Figure 3: Temperature evolution of the working lining wall (mid height), and bottom centre (HF and CF) and outer surface of steel shell during the first three thermal cycles of the steel ladle.**

Temperature distributions at the end of step 1, the end of step 2, the beginning of step 3, and the end of step 4 of the first thermal cycle are presented in Figure 4 (see Table 2 for full description of the three simulated thermal cycles and details about the four steps of each thermal cycle).

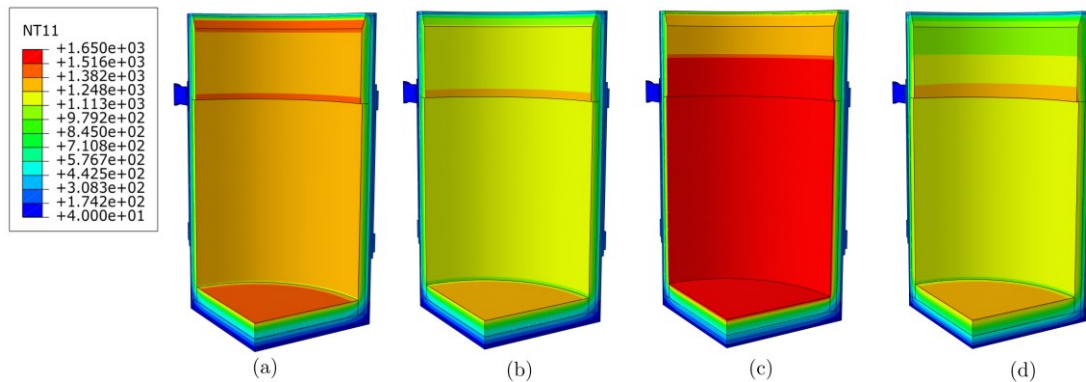


**Figure 4: Temperature distributions (in °C) at the (a) end of step 1 (point b in Figure 3), (b) end of step 2 (point c in Figure 3), (c) end of step 3 (point d in Figure 3), and (d) end of step 4 (point e in Figure 3) of the first thermal cycle of the steel ladle.**

**Table 2: Summary of the three simulated thermal cycles of the steel ladle: time period of each step and corresponding points in Figure 3.**

	First cycle		Second cycle		Third cycle	
	Duration (h)	Points	Duration (h)	Points	Duration (h)	Points
<b>Step 1</b>	6.5	a to b	1.5	e to f	1.5	i to j
<b>Step 2</b>	0.25	b to c	0.25	f to g	0.25	j to k
<b>Step 3</b>	2	c to d	2	g to h	2	k to l
<b>Step 4</b>	1	d to e	1	h to i	1	l to m

Comparisons between temperature gradient through the thickness of the steel ladle's wall and bottom at the end of step 2 and end of step 4 of the first three full steel ladle's thermal cycles are shown in Figure 5. For the second and third thermal cycles, after preheating, the temperature of the working lining is slightly higher when compared to the temperature at the end of the first preheating (points f and j as compared to point b in Figure 3). Similarly, the working lining temperature at the end of step 2 (points g and k in Figure 3) and 4 (points i and m in Figure 3) of production cycles 2 and 3 is slightly higher than that of the first thermal cycle (point c at end of step 2 and point e at end of step 4 in Figure 3). This behaviour is caused by the overall temperature increase of the ladle after the first preheating cycle (see Figure 5). It should be mentioned that during the first step of the three simulated production cycles, the inner surface temperature of the bottom is slightly higher than that of the wall. In addition, the steel shell bottom outer surface temperature is lower compared to that of the steel shell wall. This can be explained by the fact that the thickness of the working and safety lining at the bottom is higher than that at the wall.

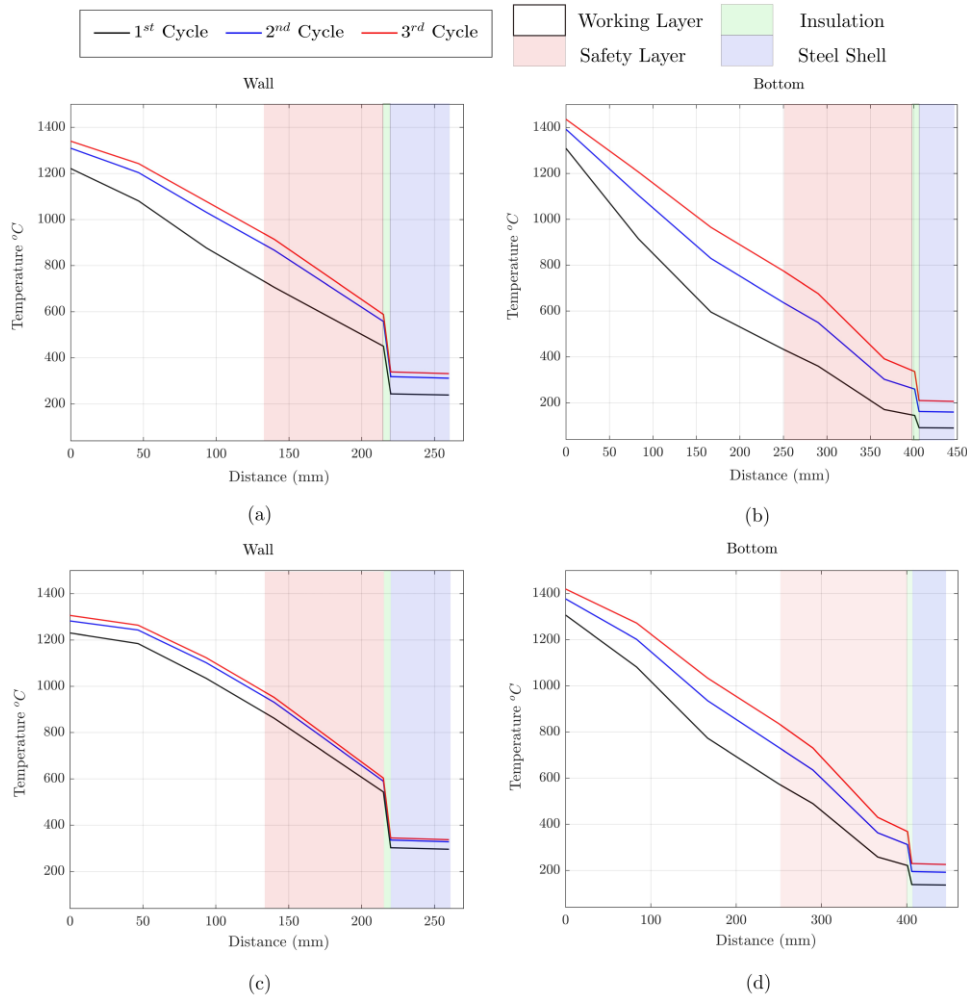


**Figure 5: Temperature gradients through the thickness of the steel ladle's wall and bottom (a and b) at end of step 2 and (c and d) end of step 4 of three full ladle's thermal cycles (see Table 2 for more details about each step of the three thermal cycles).**

## 5.2 JOINTS CLOSURE AND REOPENING

An example of the gradual closure and reopening of the joints due to temperature fluctuations during the three thermal cycles of the steel ladle is shown in Figure 6 (for a working lining without viscoplasticity - case B in Table 3). Initially (at time = 0 s), bed and head joints are open and, therefore, the working lining (bottom and wall) is in pattern O (all joints are open, see Figure 7 for more details about the four joint patterns). With the increase of the temperature, joints close gradually due to the thermal expansion of the bricks. It has been noticed that joints at the working lining hot surface (internal surface of the ladle) usually close before joints at the cold surface (surface in contact with the permanent lining) (see Figure 6-b). At almost 700 s, all joints in the hot face are closed and remain closed until the end of step 1. At the end of step 2, some joints at the outer top surface of the slag zone reopen (see Figure 6-f). This can be attributed to thermal losses, the temperature drops in this region and, therefore, the change in stress from compression to tension. These open joints close again owing to liquid steel pouring inside the ladle and the sudden increase in temperature. As the temperature drop during step 4 is higher than that during step 2, one can notice that at the end of step 4, more joints are open as compared to the number of open joints at the end of step

2 (see Figure 6-h). Therefore, waiting time (after preheating and before liquid steel tapping) is an important issue to consider when defining the duration of each step of the ladle thermal cycle. Long waiting times lead to high energy losses and may result in the opening of the joints at the wall and the bottom of the steel ladle just before tapping liquid steel in the ladle.

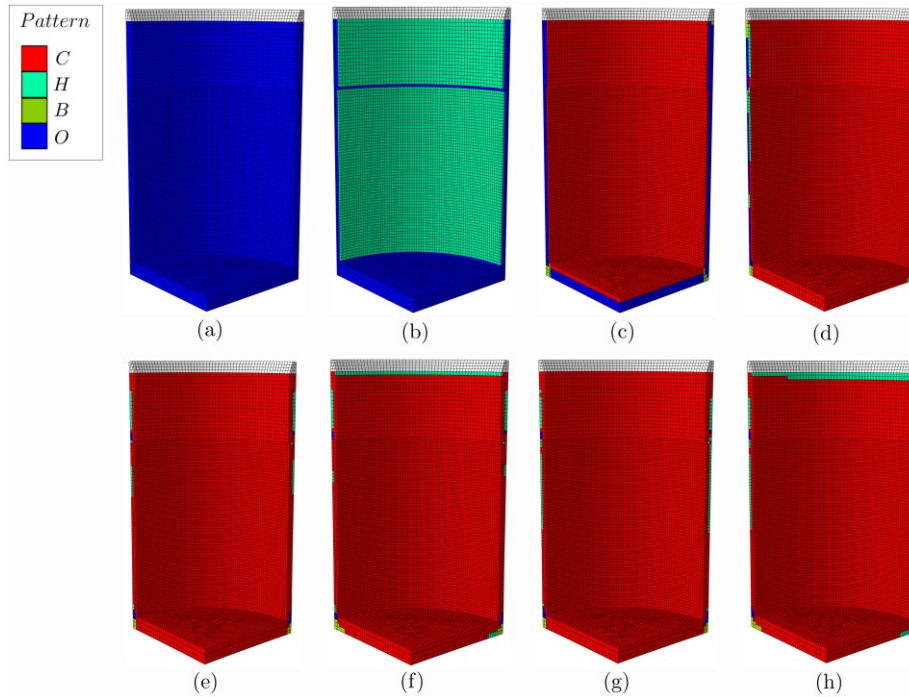


Figure 6: Gradual closure and reopening of joints due to temperature fluctuations during the first heating cycle for joint thickness of 0.1 mm (case B in

Table 3). (a) Time = 0 s (point a in Figure 3), (b) time = 0.13 h, (c) time = 0.19 h, (d) time = 0.5 h ((b) to (d) corresponds to points after point a and before point b in Figure 3), (e) time = 2.1 h (point b in Figure 3), (f) time = 6.75 h (point c in Figure 3), (g) time = 6.8 h (point d in Figure 3) and (h) time = 9.25 h (point e in Figure 3). The top zone in the working lining (in grey) is castable.

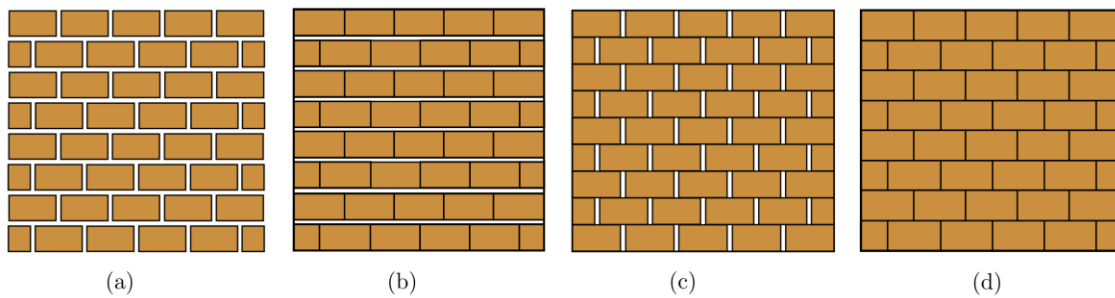


Figure 7: Schematics of possible joint patterns of refractory masonry with dry joints (a) pattern O, (b) pattern H, (c) pattern B, and (d) pattern C.

### 5.3 STRESS FIELDS

After computing the temperature distributions during the three complete thermal cycles of the ladle, some parametric studies have been carried out to investigate the impacts of dry joint thickness, joint behaviour (natural or perfect) and the employed material behaviour laws for the different layers of the ladle on the resulting thermomechanical response. Summaries of the six simulated case studies are given in

Table 3. Starting with the simplest (case (A)), increasing complexities and details are introduced to the numerical model, trying to obtain reasonable values of thermomechanical stresses. For all the case studies, the temperature distributions presented in section 5.1 were used as thermal load in the thermomechanical analysis. Therefore, the resulting differences in the thermomechanical response are caused mainly by the different constitutive models employed in the thermomechanical analysis.

**Table 3: Summary of the six simulated case studies of the ladle showing the considered joint behaviour, joint thickness and employed constitutive material models for the working, safety linings and steel shell.**

Case	Joint		Working lining	Safety lining	Steel shell
	Type	Thickness (mm)			
<b>A</b>	No Joint		Isotropic - Elastic	Isotropic - Elastic	Elastic
<b>B</b>	Perfect Joint	0.1	Orthotropic - Elastic	Isotropic - Elastic	Elastic
<b>C</b>	Perfect Joint	0.3	Orthotropic - Elastic	Isotropic - Elastic	Elastic
<b>D</b>	Perfect Joint	0.5	Orthotropic - Elastic	Isotropic - Elastic	Elastic
<b>E</b>	Perfect Joint	0.1 - higher values of Young's modulus	Orthotropic - Elastic	Isotropic - Elastic	Elastic
<b>F</b>	Natural Joint	0.5	Orthotropic - Elastic	Isotropic - Elastic	Elastic
<b>G</b>	Natural Joint	0.5	Orthotropic - Elastic - Viscoplastic	Orthotropic - Elastic - Damageable	Elastic - Plastic

In previous work of the author [4], it has been shown that the linings are subjected to a biaxial stress state and the out of plane stresses are negligible as compared to the in-plane stresses. Therefore, the comparisons of the resulting thermomechanical stresses (for the six simulated cases) were carried out in terms of resulting in-plane stresses at mid height of the wall HF (2500 mm), the centre of the bottom HF ( $R = 0$  mm) and von Mises stresses in the steel shell outer surfaces (mid height of the wall and bottom centre).

### 5.3.1 Impacts of dry joints thickness

In the case A, the dry joints in the working lining and the mortar joints in the safety linings were neglected. All the layers of the ladle were modelled using simple isotropic linear elasticity. This case is considered as the reference case. To investigate the impacts of dry joints thickness on the resulting thermomechanical stresses, three cases were simulated (B, C and D). The joints behaviour was considered as perfect (i.e. gradual closure of joints and increase of effective stiffness with joints closure were neglected). As mentioned in references [4], [6], [8], perfect joints with almost controlled thickness can be artificially generated by inserting cardboard spacers between the contact surfaces of the bricks and, in this case, joints can be considered as either open or closed. Therefore, the initial mechanical behaviour of the working lining is orthotropic (due to the presence of open joints). To avoid the contribution of viscoplasticity, plasticity of the steel shell, the damage of mortar joints (in the safety linings) and for better understanding of the impact of joints thickness on resulting thermomechanical stresses, the mechanical behaviours of the other layers were considered as isotropic and purely elastic.

Time variations of the thermal stresses in the hot face of the wall (middle,  $H = 2500$  mm) and bottom (centre,  $R = 0$  mm) of the working lining for different values of bed and head joint thickness (cases B, C and D), as well as the isotropic representation of the masonry (case A), during the first three thermal cycles are shown in Figure 8. In general, it has been observed that the resulting thermal stresses increase with the increase in temperature, decrease with the increase of joint thickness, and their trends are similar to those of the temperature during the four steps of the ladle thermal cycle. In addition, the isotropic assumption of mortarless masonry leads to an overestimation of resulting thermal stresses.

During the first step, thermal stresses increase with the increase in temperature and thermal expansion of the bricks. Then (during step 2), they decrease slightly due to the temperature decrease and contraction of the bricks. The maximum value of thermal stresses is reached when liquid steel is tapped in the steel ladle. This is because of the sudden increase in temperature. During step 4, they decrease again with the decrease in temperature. Finally, this trend is repeated. It can be noted that the hot face is under high compressive stresses. This result may be explained by the fact that the temperature of the hot face is higher than the temperature of the other layers and it tends to expand faster than the safety layer, insulation layer and the steel shell.

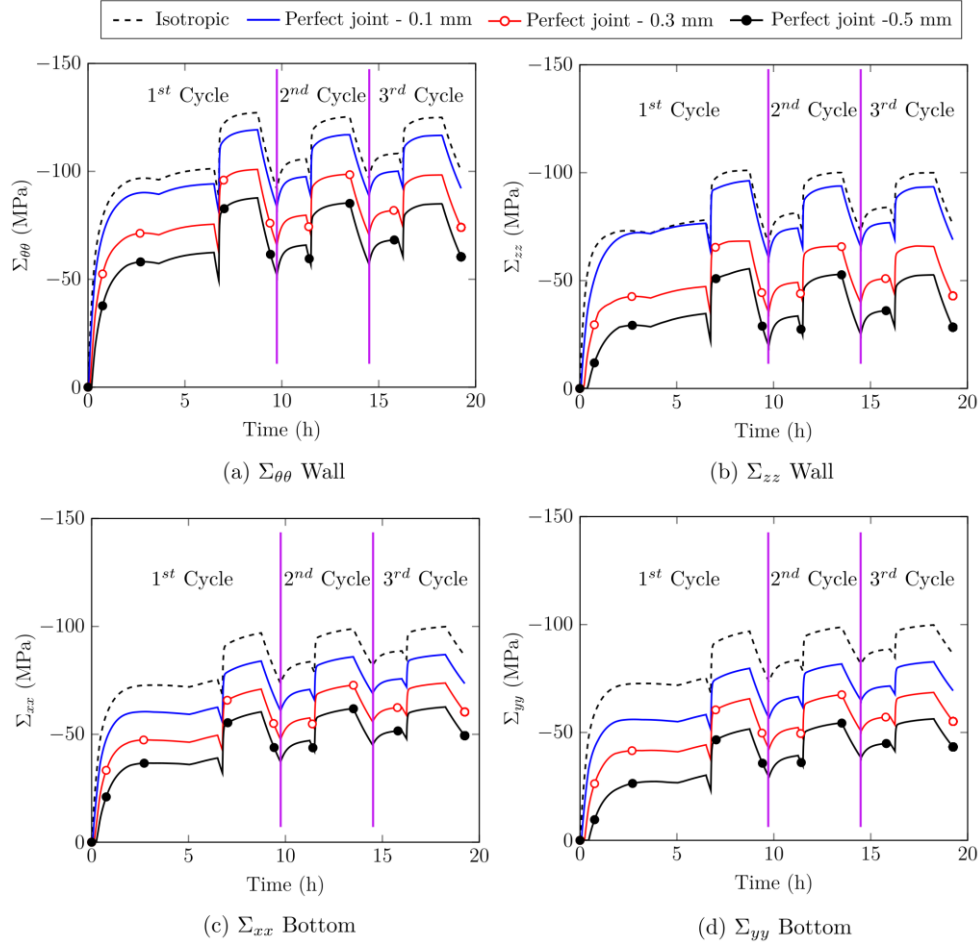


**Figure 8: (a and b) Time variations of the thermal stresses at the wall surface (HF) and (c and d) bottom surface (HF) of the working lining for different values of bed and head joint thickness during the first three thermal cycles of the steel ladle.**

Time variations of the von Mises stresses in the steel shell (bottom and wall) for different values of bed and head joint thickness (cases B, C and D), as well as isotropic representation of the masonry (case A) are given in Figure 9. Overall, it has been observed that the von Mises stresses increase with the increase in temperature, decrease with the increase of joint thickness, and their trends are similar to those of the temperature during the four steps of the ladle thermal cycle. Based on the above results, it can be concluded that increasing joint thickness leads to a decrease in the resulting thermal stresses in the bottom and the wall of the working lining, as well as the steel shell. Increasing joint thickness allows the bricks to expand freely (until closure of joints), resulting in lower values of thermal stresses. After the closure of joints, thermal stresses increase at higher rates. This phenomenon can be noticed in Figure 8 - b and d for joint thickness 0.5 mm. In the first 500 s, as joints thickness is higher than zero during this period (therefore, considered open), the values of the resulting thermal stresses are very small (almost zero).

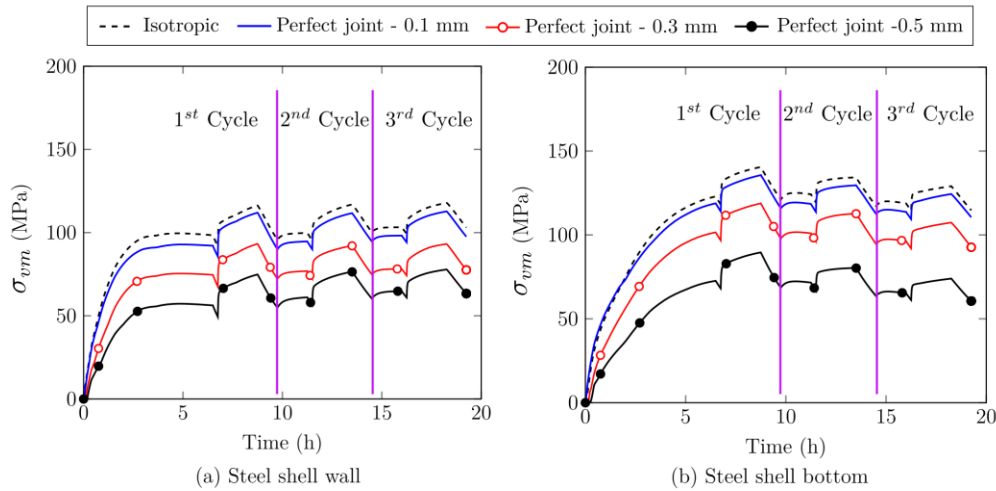


**Figure 9: Time variations of the von Mises stresses in the (a) wall and (b) bottom of the steel shell for different values of bed and head joint thickness during the first three thermal cycles of the steel ladle.**

### 5.3.2 Impact of Young's modulus

To investigate the impact of the values of Young's modulus of the working lining on the resulting thermomechanical stresses, a numerical simulation (case E) with higher values of Young's modulus has been carried out. The higher and reference values of Young's modulus correspond to those from mechanical tests and ultrasonic technique as reported in deliverable 3.6 and given in Figure 10. For the blue line in the figure, the values of Young's modulus, for temperatures above 1300 °C and below 800 °C, were obtained by fitting the curve.

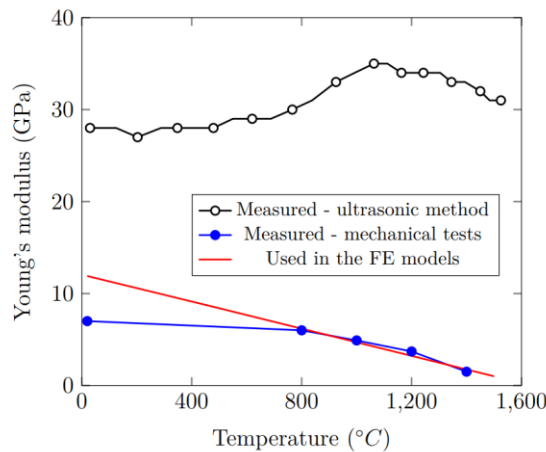


**Figure 10: Young's modulus of alumina spinel measured by ultrasonic technique and mechanical tests.**

Time variations of the thermal stresses in the HF of the wall (middle H = 2500 mm) and bottom (centre, R = 0 mm) of the working lining with higher values of Young's modulus (cases E, joint thickness = 0.1 mm), as well as reference values of Young's modulus (case B, joint thickness = 0.1 mm), during the first three heating cycles are shown in Figure 11. It can be observed that increasing the values of Young's modulus leads to an increase in the resulting thermomechanical stresses. Similar observations were also noticed for the von Mises stresses in the steel shell.

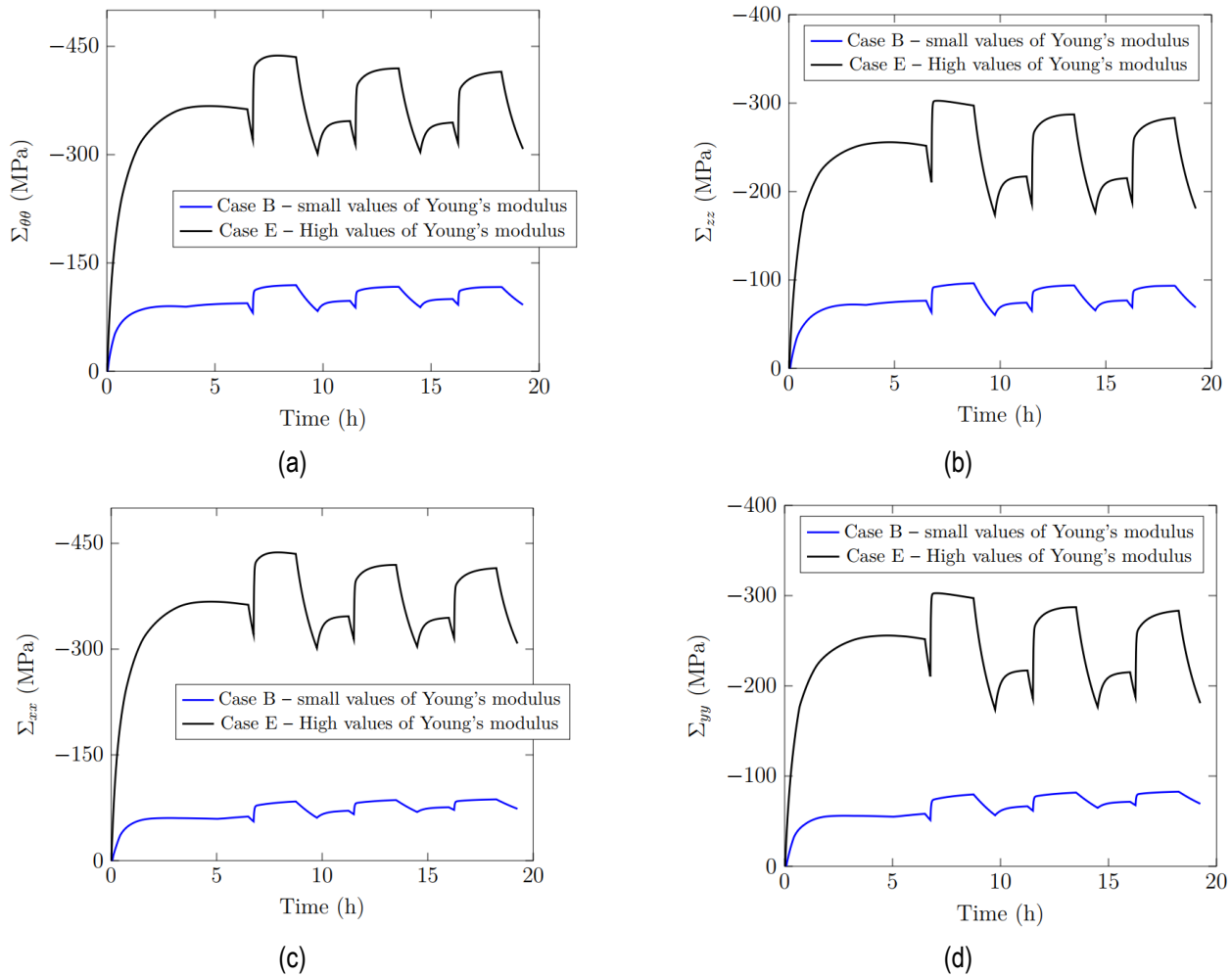


**Figure 11: Time variations of the resulting thermomechanical stresses in the in the wall (a and b) and the bottom (c and d) in directions (a)  $\theta\theta$ , (b)  $zz$ , (c)  $xx$  and (d)  $yy$ .**

### 5.3.3 Impacts of dry joints behaviour

In most cases, cardboard spacers are not used while building the linings and natural joints are generated between the bricks by the dimensional, shape tolerances and surface roughness of the bricks. Therefore, a numerical simulation (case F) with natural joint behaviour was carried out. For natural joints, as shown in [6], the gradual closure of joints and the related gradual increase in the effective stiffness of the masonry with the closure of joints are considered. Case F may help in understanding the impacts of joint behaviour on the resulting thermomechanical stresses. The considered joint behaviour is similar to that presented in deliverable 3.6. Indeed, the real joints behaviour of the tapered, shaped bricks (used for building the working lining) could be different from that of the cuboid bricks presented in deliverable 4.3. However, based on the available data, the assumption of similar joints behaviour is acceptable.

Time variations of the thermal stresses in the HF of the wall (middle  $H = 2500$  mm) and bottom (centre,  $R = 0$  mm) of the working lining for bed and head joints with natural behaviour (cases F), as well as perfect joints behaviour (cases C and D), during the first three heating cycles are shown in Figure 12. Time variations of the von Mises stresses in the wall and the bottom of the steel shell for joints with perfect and natural behaviour during the first three thermal cycles of the steel ladle are given in Figure 13. In general, for masonry with natural joints behaviour, similar trends (as cases A, B, C and D) of the resulting thermal stresses in the working lining and the steel shell can be observed from the figures.

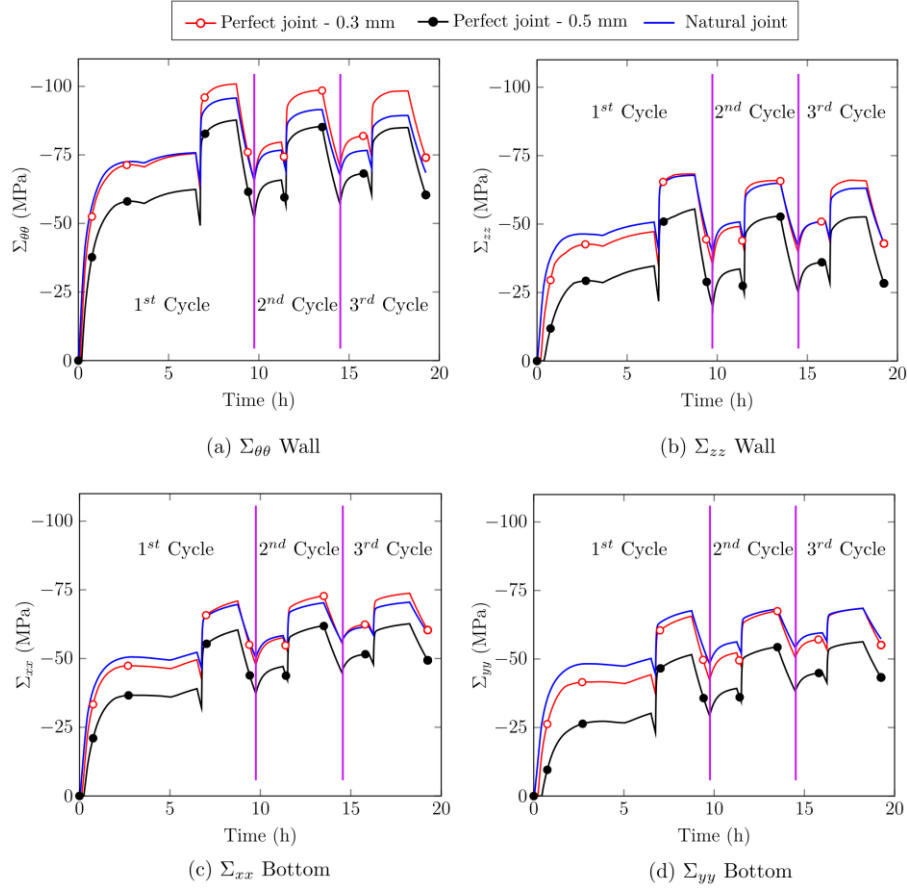


**Figure 12: (a and b) Time variations of the thermal stresses in the wall HF and (c and d) bottom HF of the working lining for joints with perfect and natural behaviour during the first three thermal cycles of the steel ladle.**

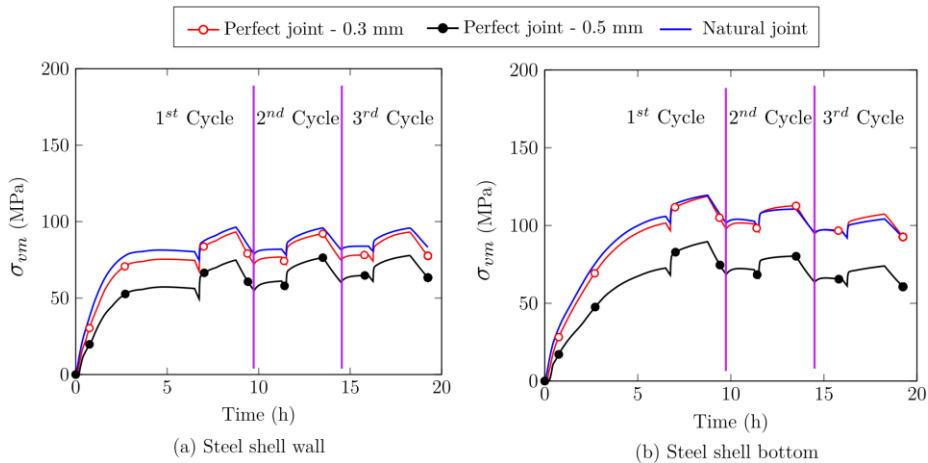


**Figure 13: Time variations of the von Mises stresses in the (a) wall and (b) bottom of the steel shell for joints with perfect and natural behaviour during the first three thermal cycles of the steel ladle.**

For the same joint thickness (0.5 mm), using masonry with natural joints behaviour results in higher values of resulting thermomechanical stresses. This can be attributed to that in the case of perfect joint, the in-plane effective stiffness of the masonry is almost zero and remains very small until full closure of joints (i.e. there is a sudden jump in the effective stiffness when full closure happens and the values of resulting stresses are almost zero before full closure of joints). On the other hand, for natural joints, the in-plane effective stiffness increases gradually with the gradual closure of joints (due to the increase of the normal and shear stiffnesses of the joint with their gradual closure, see Figure 14). The in-plane effective stiffness reaches the maximum value (same as that of the brick) when joints are fully closed. Based on these results, it can be recommended that decreasing the dimension errors of the bricks and generating artificial joints using cardboard spacers could be better in terms of resulting

thermomechanical stresses. Moreover, natural joints (caused mainly by the dimension errors of the bricks) leads to stress concentrations at the middle of the bricks and a significant reduction in the load bearing capacity of the masonry [6].

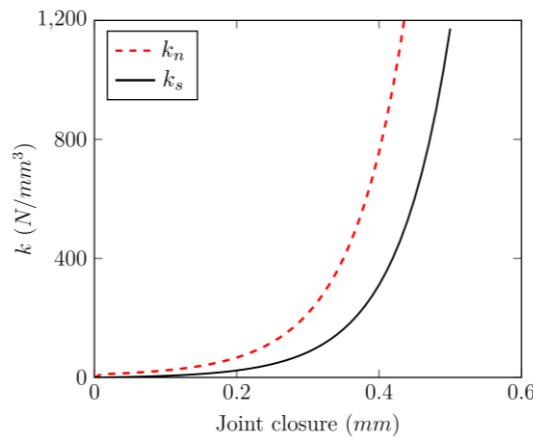
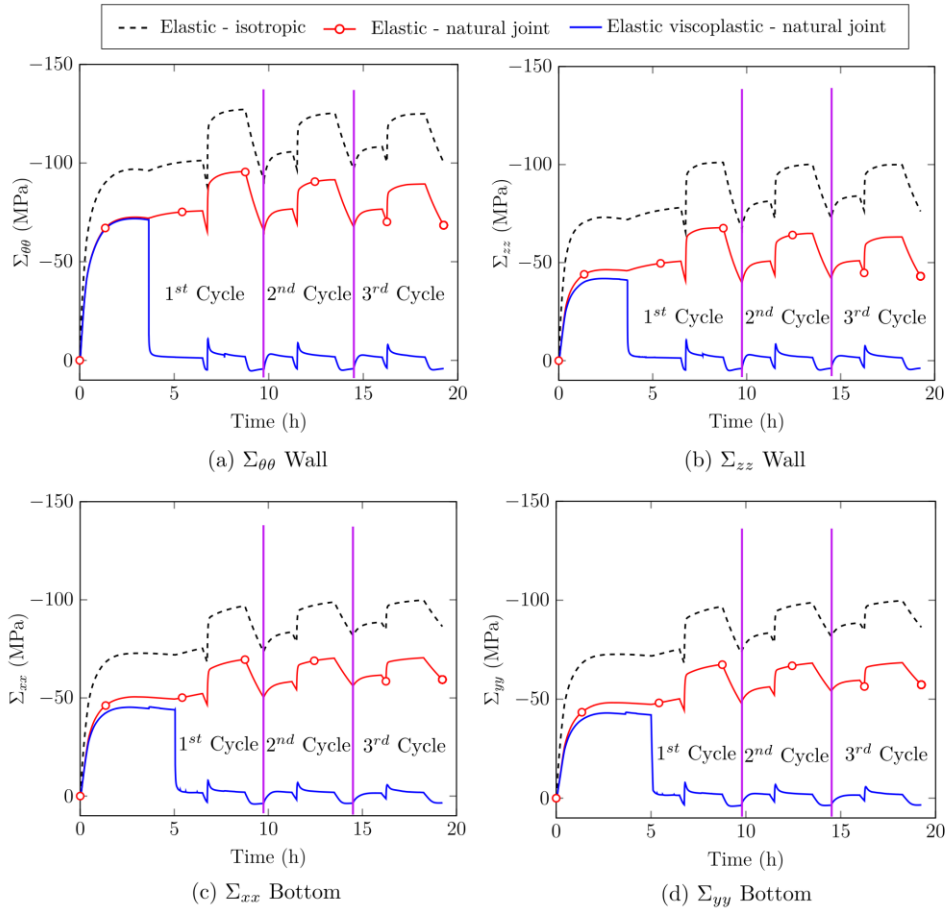


Figure 14: Variations of the normal and shear stiffnesses of the natural joints with gradual joints closure [6].

### 5.3.4 Linings with elastic-viscoplastic behaviour

In the last case study (case G), the working and safety linings of the steel ladle are modelled using more accurate behaviour laws. The orthotropic elastic viscoplastic behaviour of refractory masonry with dry joints is considered. The von Mises plasticity theory was used to model the plastic behaviour of the steel shell. One of the main challenges in this simulation is related to the lack of important data to define the temperature and corresponding yield stress at which the behaviour of the masonry changes from elastic-to-elastic viscoplastic (creep starting temperature and corresponding yield stress). These data should be determined experimentally and should be available to build a realistic and accurate numerical model. In the case of refractories and for temperatures above or equal to 1000 °C, it has been usually assumed that the yield stress is equal to zero [9]–[11] (i.e. creep starts at any value of stress). In the case of alumina spinel, no creep parameters, creep starting temperature and corresponding yield stress data are available for temperatures below 1300 °C. It has been shown that, in deliverable 3.6, at 1200 °C and under 6 MPa compressive load, the creep strain was insignificant as compared to higher temperatures. However, this conclusion was based on lower value of applied compressive stress as compared to the values of stresses observed here (steel ladle simulation) and the ultimate compressive stress of the material (25 MPa). Therefore, due to the lack of the required data, it has been assumed that the creep starting temperature is 1200 °C (same creep parameters as 1300 °C) and the yield stress was set to zero.

Time variations of the thermal stresses in the hot face of the wall (middle, H = 2500 mm) and bottom (centre, R = 0 mm) of the working lining for case F and G, as well as the isotropic elastic representation of the masonry (case A), during the first three thermal cycles of the ladle are shown in Figure 15. In general, it has been observed that, in the first four hours, the resulting compressive thermal stresses in the case F are similar to that in the case G. Next, in the case G, the stresses decreased sharply (when the temperature reached the set value of creep starting temperature) to around -5 MPa due to stress relaxation. Then, they remained at this value until the end of the preheating stage. During the second step of the first thermal cycle and with the decrease of the temperature, the stresses changed from compressive to tensile. This can be attributed to the contraction of the bricks with the decrease in the temperature. By the start of the third step (liquid steel tapping), the stresses changed the sign again from tensile to compressive stresses due to the sudden increase in the temperature. During the same step, a decay in the stresses was observed due to stress relaxation. Finally, during the fourth step, the stresses changed from compressive to tensile due to heat losses and contraction of the bricks. The same trends have been observed for the second and third thermal cycles of the ladle.



**Figure 15: Variations of the stresses (in the HF of the wall and the bottom) and comparisons of different constitutive material models including viscoplasticity.**

The stress levels obtained here are still unrealistic because they are higher than the ultimate compressive strength of the material (25 MPa at 1000 °C). The creep starting temperature and corresponding yield stress used in the model are other important factors that impact the resulting thermomechanical stresses during the first four hours. For example, lowering the creep initiation temperature to 800 °C and having the corresponding creep parameters and yield stress would result in a reduction in the thermomechanical stresses. Moreover, the sudden decrease of stresses (once reaching the creep temperature set value) may not occur in reality. Including the creep impacts at lower temperatures would lead to gradual decrease of stresses instead of the sudden decrease noticed here. However, this requires experimental characterization and inverse identification of the creep parameters of the material at lower temperatures. Future experimental studies to investigate the creep behaviour at lower temperatures and include its effects on the numerical model are planned.

The change of stress sign from compressive to tensile leads to reopening of dry joints in the HF of the wall and the bottom. On the other hand, the change of its sign from tensile to compressive leads to re-closure of the reopened joints. More explanations and insights are given for the first and second changes of stress sign reported in Figure 15 will be discussed now. Figure 16 shows the joint patterns in the working lining and the bottom at the end of step 2 (first temperature drop after first preheating), 500 seconds from the beginning of step 3 (first liquid steel tapping into the ladle - sudden temperature increase) and end of step 4 (temperature drop due to teeming liquid steel out of the ladle and waiting time for linings check and repair). It can be seen that, with the temperature drop and change of stress sign, almost all joints in the HF of the bottom and the wall reopened (see Figure 16- a). Then, the reopened joints close again when liquid steel is tapped into the ladle (see Figure 16-b). Finally, with the second temperature decrease and the change of stress from compression to tension, joints in the HF reopen (see Figure 16-c). These described openings and closures of joints during the first and second changes of stress sign were noticed for each change of stress sign shown in Figure 15. In the safety lining, damage of bed or head or both mortar joints was observed (see Figure 17). The damaged joints were mainly located in the top and the bottom zones of the wall of the safety linings (see Figure 18 for more details about the four joint patterns). The re-closure of damaged mortar joints under compressive loads was not included in the numerical model, because this requires further experimental studies of the mortar joints behaviour during re-closure and further developments of the numerical model that are planned to be carried out in the future.

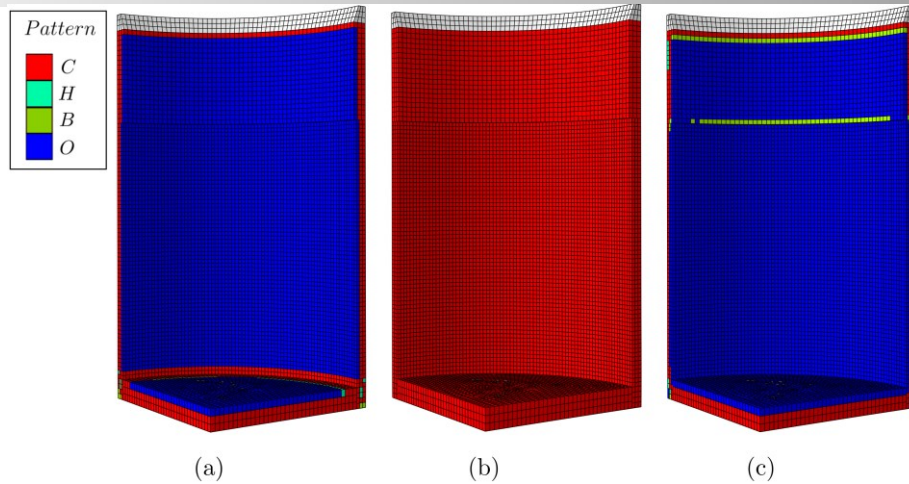


Figure 16: Joints reopening and closure in the wall and the bottom (working lining) of the steel ladle due to temperature fluctuations and the change of stress sign (from compressive to tensile and vice versa) at (a) the end of the second step, (b) the beginning of the third step and (c) the end of the fourth step of the first thermal cycle of the steel ladle.

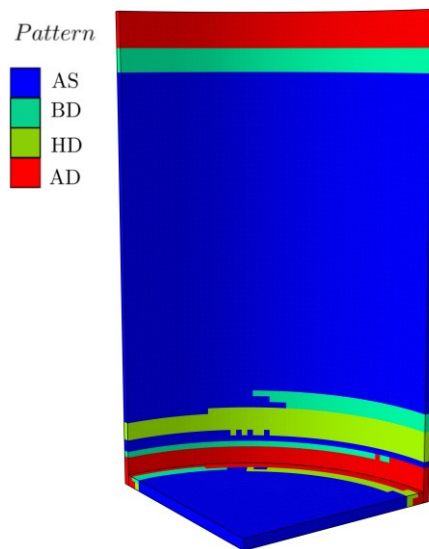


Figure 17: Damage of mortar joints in the safety lining wall.

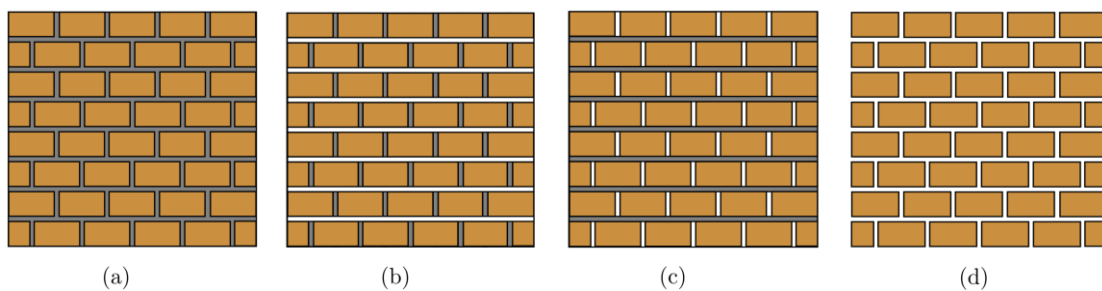
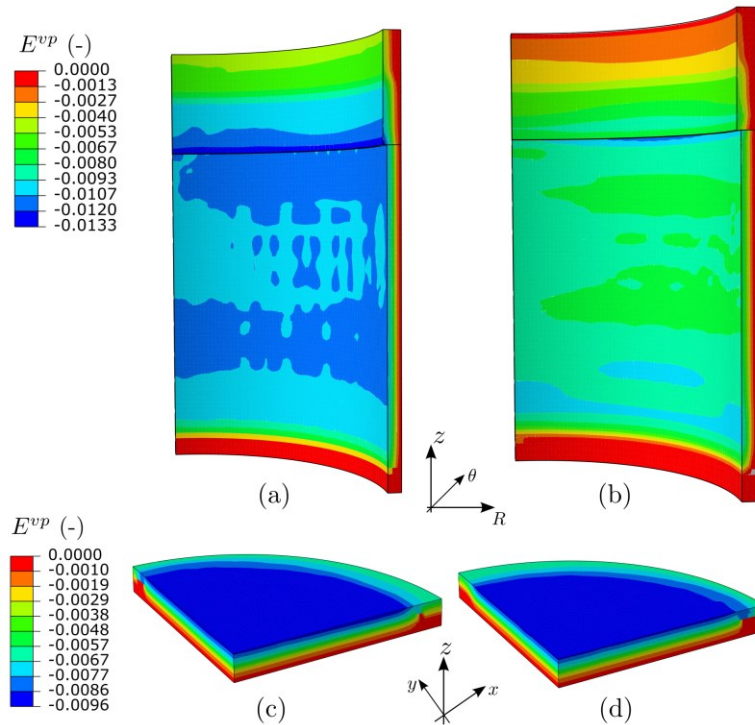


Figure 18: Schematics of possible joint patterns of masonry structure with mortar joints (a) pattern AS, (b) pattern BD, (c) pattern HD, and (d) pattern AD.

The in-plane viscoplastic strains, in the case F, in the wall (in  $\theta\theta$  and  $zz$  directions) and the bottom (in  $xx$  and  $yy$  directions) of the working lining of the steel ladle by the end of the three simulated thermal cycles are presented in Figure 19. It can be seen that the highest values of viscoplastic strains are located in the HF of the wall in the  $\theta\theta$  direction. This is due to the fact that in Figure 15 the highest values of the computed thermomechanical stresses are normally in the same direction. Moreover, the viscoplastic strains in the CF of the wall and the bottom are almost zero. This can be attributed to that the calculated temperatures of the CF

of the bottom and the wall (presented in Figure 3) were always below the set value of creep initiation temperature (1200 °C). No viscoplasticity was noticed in the safety lining because its temperature, again, was below the set value of creep initiation temperature.



**Figure 19: Viscoplastic strains fields in the wall (a and b) and the bottom (c and d) in directions (a)  $\theta\theta$ , (b)  $zz$ , (c)  $xx$  and (d)  $yy$  by the end of the three simulated thermal cycles of the steel ladle.**

Time variations of von Mises stresses in the steel shell wall (middle,  $H = 2500$  mm) and bottom (centre,  $R = 0$  mm) for cases F and G, as well as the isotropic elastic representation of the masonry (case A), during the first three heating cycles are shown in Figure 20. Significant reductions of von Mises stresses were noticed four hours after the first preheating (corresponds to the sharp reduction in the stresses of the HF of the bottom and the wall).

It should be noted that changing the constitutive material models of the different layers of the ladle and the steel shell leads to a change in the von Mises stress distribution. Therefore, comparing the von Mises stress variations with time of a specific point may result in less accurate conclusion. A judicious comparison could be made in terms of the maximum value of von Mises stress in the entire steel shell. The maximum value of von Mises stresses in the steel shell, obtained numerically, was always located in the barrel zone (top zone of the steel shell wall) of the steel ladle. In real steel ladles, damage and high deformation of this zone were also observed (see Figure 21). A comparison between the maximum value of von Mises stresses for the seven studied cases is presented in Figure 22. The yield and ultimate tensile strength of steel are 250 and 400 to 550 MPa, respectively. The highest value of von Mises stress was obtained using the higher values of Young's modulus for the working lining (case E), followed by the isotropic representation of the working linings (case A). On the other hand, the lowest value was obtained when more accurate material models of the working, the safety linings and the steel shell were employed. In addition, it can be seen that increasing the dry joints thickness leads to a decrease in the maximum value of Mises stress in the barrel zone.

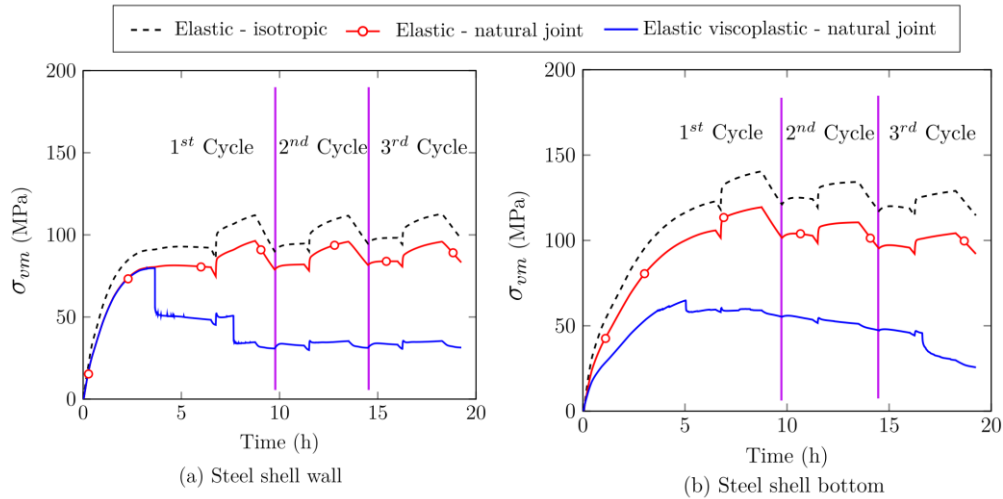


**Figure 20: Time variations of von Mises stresses in the hot face of the steel shell wall and bottom for cases E, F and A during the first three thermal cycles of the steel ladle.**

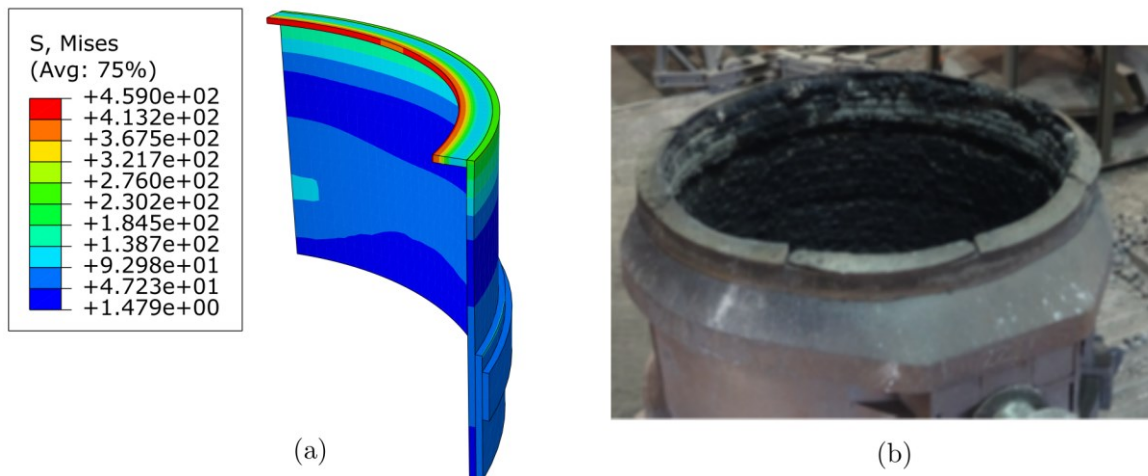


**Figure 21: (a) Example of von Mises stress (in MPa, case A) in the barrel zone of the steel shell and (b) damage and permanent deformation of the top flange of a real steel ladle.**

Based on the above results and discussions, it can be concluded that either the isotropic assumption of mortarless masonry or orthotropic elastic assumption leads to overestimation of resulting thermal stresses. In addition, it can be concluded that the most critical stage of the ladle thermal cycle is the first preheating. Using a material with lower values of coefficient of thermal expansion could help in reducing the resulting thermomechanical stresses of the ladle. Further parametric studies to investigate the usage of perfect joints with an optimum thickness (combined with viscoplasticity at lower temperatures, below 1200 °C) on the resulting thermal stresses are planned in future work. Indeed, the impacts of creep at lower temperatures, corrosion, damage, wear and thermal shock could change these conclusions and add greater insights on the thermomechanical response of the ladle.

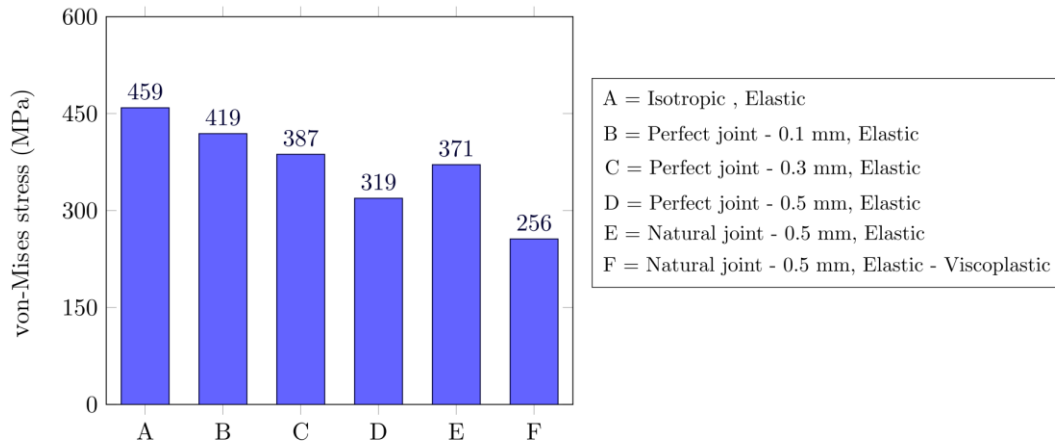


Figure 22: Maximum values of von Mises stress in the steel shell obtained from the six simulated case studies.

## 6 Conclusion

In the present work, three-dimensional coupled sequential thermomechanical analysis of a steel ladle has been carried out. The working lining and the bottom of the ladle have been replaced by an equivalent material model that takes into account the closure and reopening of joints due to cyclic thermal or mechanical loading/unloading. The temperature distribution of the steel ladle has been computed and used as a thermal load for the thermomechanical analysis. The thermomechanical model enables the visualisation of the gradual closure and reopening of joints during the complete thermal cycle of the ladle. The impacts of joint thickness, joint behaviour, constitutive material models used for the different linings of the ladle and the steel shell on the resulting thermomechanical stresses have been studied. The following conclusions can be drawn:

- With the increase in temperature, dry joints close gradually due to the thermal expansion of the bricks. Joints at the working lining hot surface close faster than joints at the cold surface.
- The temperature drop during the waiting time results in the opening of some joints at the outer top surface of the slag zone. Moreover, waiting time is an important issue to consider when defining the time period of each step of the ladle thermal cycle. Long waiting times lead to high energy losses and may result in the opening of joints at the wall and the bottom of the steel ladle just before tapping liquid steel in the ladle.
- Resulting thermal stresses in the hot face increase with the increase in temperature, and their trends are similar to those of the temperature during the four steps of the thermal ladle heating cycle.
- Increasing joint thickness leads to a decrease in the resulting thermal stresses in the bottom and the wall of the working lining, as well as in the steel shell.
- For the same joint thickness, using masonry with natural joint behaviour results in higher values of resulting thermomechanical stresses as compared to perfect joint.
- Either the isotropic assumption of mortarless masonry or orthotropic elastic assumption leads to an overestimation of resulting thermal stresses.
- The inclusion of the viscoplasticity to the numerical model has a significant impact on the resulting thermomechanical stresses. A change of stress sign from compression to tension and opening/closure of dry joints in the HF of the working linings was observed. Moreover, lower values of the thermomechanical stresses were obtained when using more accurate behaviour laws for the different layers in the steel ladle.

## 7 References

- [1] J. Brulin *et al.*, "Methodology for brick/mortar interface strength characterization at high temperature," *Constr. Build. Mater.*, vol. 265, p. 120565, 2020, doi: 10.1016/j.conbuildmat.2020.120565.
- [2] M. F. Santos *et al.*, "Enhanced numerical tool to evaluate steel ladle thermal losses," *Ceram. Int.*, vol. 44, no. 11, pp. 12831–12840, 2018, doi: 10.1016/j.ceramint.2018.04.092.
- [3] A. Hou, S. Jin, H. Harmuth, and D. Gruber, "A Method for Steel Ladle Lining Optimization Applying Thermomechanical Modeling and Taguchi Approaches," *Jom*, vol. 70, no. 11, pp. 2449–2456, 2018, doi: 10.1007/s11837-018-3063-1.
- [4] M. Ali, T. Sayet, A. Gasser, and E. Blond, "Transient thermo-mechanical analysis of steel ladle refractory linings using

- mechanical homogenization approach," *Ceramics*, vol. 3, no. 2, pp. 171–189, 2020, doi: 10.3390/ceramics3020016.
- [5] Y. A. Cengel and A. J. Ghajar, *Heat and mass transfer: fundamentals and applications*. McGraw-Hill Education, 2007.
- [6] M. Ali, "Nonlinear thermomechanical modelling of refractory masonry Linings, PhD thesis," University of Orléans - France, 2021.
- [7] J. L. Xia and T. Ahokainen, "Transient flow and heat transfer in a Steelmaking ladle during the holding period," *Metall. Mater. Trans. B Process Metall. Mater. Process. Sci.*, vol. 32, no. 4, pp. 733–741, 2001, doi: 10.1007/s11663-001-0127-2.
- [8] M. Ali, T. Sayet, A. Gasser, and E. Blond, "Computational homogenization of elastic-viscoplastic refractory masonry with dry joints," *Int. J. Mech. Sci.*, vol. 196, p. 106275, 2021, doi: 10.1016/j.ijmecsci.2021.106275.
- [9] S. Jin, H. Harmuth, and D. Gruber, "Compressive creep testing of refractories at elevated loads-Device, material law and evaluation techniques," *J. Eur. Ceram. Soc.*, vol. 34, no. 15, pp. 4037–4042, 2014, doi: 10.1016/j.jeurceramsoc.2014.05.034.
- [10] E. Blond, N. Schmitt, F. Hild, P. Blumenfeld, and J. Poirier, "Modelling of high temperature asymmetric creep behavior of ceramics," *J. Eur. Ceram. Soc.*, vol. 25, no. 11, pp. 1819–1827, 2005, doi: 10.1016/j.jeurceramsoc.2004.06.004.
- [11] L. Teixeira, J. Gillibert, T. Sayet, and E. Blond, "A creep model with different properties under tension and compression — Applications to refractory materials," *Int. J. Mech. Sci.*, vol. 212, p. 106810, 2021, doi: 10.1016/j.ijmecsci.2021.106810.